JBC Papers in Press. Published on November 3, 2009 as Manuscript M109.050906
The latest version is at http://www.jbc.org/cgi/doi/10.1074/jbc.M109.050906

Conditional Disruption of *Pkd1* in Osteoblasts Results in Osteopenia due to Direct Impairment of Bone Formation

Zhousheng Xiao, Shiqin Zhang, Li Cao, Ni Qiu, Valentin David, L. Darryl Quarles
The Kidney Institute, University of Kansas Medical Center, Kansas City, KS, USA

Running title: PC1 Regulates Osteoblast Function via PI3K/Akt/Gsk3β

Address correspondence to: L. Darryl Quarles, M.D., University of Kansas Medical Center, MS 3018, 3901 Rainbow Boulevard, 6018 Wahl Hall East, Kansas City, KS 66160, Tel. 913-588-9252; Fax: 913-588-9251; E-mail: dquarles@kumc.edu

Polycystin-1 (Pkd1), the disease-causing gene for ADPKD, is widely expressed in various cell types, including osteoblasts, where its function is unknown. Although global inactivation of Pkd1 in mice results in abnormal skeletal development, the presence of polycystic kidneys and perinatal lethality confound ascertaining the direct osteoblastic functions of Pkd1 in adult bone. To determine the role of Pkd1 in osteoblasts, we conditionally inactivated Pkd1 in postnatal mature osteoblasts by crossing *Osteocalcin* (*Oc*)-Cre mice with floxed *Pkd1* (*Pkd1*$^{\mathrm{flox/m1Bei}}$) mice to generate conditional heterozygous (*Oc*-Cre;*Pkd1*$^{\mathrm{flox/+}}$) and homozygous (*Oc*-Cre;*Pkd1*$^{\mathrm{flox/m1Bei}}$) *Pkd1*-deficient mice. Cre-mediated recombination (*Pkd1*$^{\Delta\mathrm{flox}}$) occurred exclusively in bone. Compared to control mice, the conditional deletion of *Pkd1* from osteoblasts resulted in a gene-dose dependent reduction in bone mineral density, trabecular bone volume and cortical thickness. In addition, mineral apposition rates and osteoblast-related genes expression, including *Runx2*-II, *Osteocalcin*, *Osteopontin*, and *Bone Sialoprotein,* were reduced proportionate to the reduction of *Pkd1* gene dose in bone of *Oc*-Cre;*Pkd1*$^{\mathrm{flox/+}}$ and *Oc*-Cre;*Pkd1*$^{\mathrm{flox/m1Bei}}$ mice. Primary osteoblasts derived from *Oc*-Cre; *Pkd1*$^{\mathrm{flox/m1Bei}}$ displayed impaired differentiation and suppressed activity of the PI3K-Akt-Gsk3β-β-catenin signaling pathways. The conditional deletion of *Pkd1* also resulted in increased adipogenesis in bone marrow and in osteoblast cultures. Thus, Pkd1 directly functions in osteoblasts to regulate bone formation.

Polycystin-1 (PC1) is a highly conserved, receptor-like multi-domain membrane protein widely expressed in various cell types and tissues (1,2). Mutations of human *PKD1* cause Autosomal Dominant Polycystic Kidney Disease (ADPKD) (3,4). The genetics of ADPKD is complex, since it is widely held that inactivation of the normal copy of the *PKD1* gene by a second somatic mutation in conjunction with the inherited mutation of the other allele are required for renal cyst formation, which occurs in only a subset of the dually affected tubules (5). Although primarily affecting the kidney, ADPKD is also a multisystem disorder (6,7). Extrarenal manifestations include intracranial and aortic aneurysms, and cystic disease of liver and pancreas (8-11). The biological functions of PC1 are poorly defined in some tissues that express *PKD1* transcripts, such as bone. Indeed, the absence of clinically demonstrable skeletal abnormalities in patients with ADPKD initially delayed the investigation of PKD1 function in bone. The apparent lack of abnormalities in other tissues expressing PC1 may arise because of differences in the frequency of a second hit somatic mutation, the presence of other modifying factors that may compensate for lack of PC1 function in other organs (12), or failure to detect more subtile phenotypes. For example, lung was not thought to be affected by *PKD1* mutations until CT scans of lungs of ADPKD patients showed a 3-fold increase in the prevalence of bronchiectasis compared to controls (13).

Pkd1 is highly expressed in bone and several mouse models with inactivating mutations of *Pkd1* have skeletal abnormalities in the setting of polycystic kidney disease and embryonic lethality (6,7,14-16). Most recently, however, the heterozygous *Pkd1*$^{\mathrm{m1Bei}}$ mouse, which has an inactivating mutation of *Pkd1* and survives to adulthood without polycystic kidney disease, has been shown to develop osteopenia and impaired osteoblastic differentiation (17,18), suggesting that Pkd1 may function in bone. Since homozygous *PKD1*/*Pkd1* mutations in humans and mice are lethal, and most of the existing models are globally *Pkd1* deficient, the significance of inactivation of Pkd1 in osetoblasts remains uncertain, and the bone changes might reflect an indirect effect due to loss of PKD1/Pkd1 in the kidney or other tissues.

In the current study, to determine if Pkd1 in osteoblasts has a direct function in regulating postnatal skeletal functions, we used mouse genetic approaches to conditionally delete *Pkd1* in osteoblasts. We demonstrate that conditional deletion of *Pkd1* from osteoblasts of heterozogyous *Pkd1*$^{m1Bei/+}$ mutant mice in defective osteoblast-function *in vivo* and *in vitro*, and osteopenia, indicating that Pkd1 has a direct role to regulate osteoblast function and skeletal homeostasis.

EXPERIMENTAL PROCEDURES

Mice — We obtained the floxed *Pkd1* mice from Dr. Gregory Germino at Johns Hopkins University (19) and *Osteocalcin* (*Oc*)-Cre mice from Dr. Thomas Clemens at University of Alabama (20). The *Pkd1*^{m1Bei} heterozygous mice were available in our laboratory as previously described (18). These mice were bred and maintained on a C57BL/6J background. At first, we created double heterozygous *Oc*-Cre;*Pkd1*$^{m1Bei/+}$ mice and homozygous *Pkd1*$^{flox/flox}$ mice. Then double heterozygous *Oc*-Cre;*Pkd1*$^{m1Bei/+}$ mice were mated with homozygous *Pkd1*$^{flox/flox}$ mice to generate excised floxed *Pkd1* heterozygous (*Oc*-Cre;*Pkd1*$^{flox/+}$) and null mice (*Oc*-Cre;*Pkd1*$^{flox/m1Bei}$ or *Pkd1*$^{Oc\text{-}cko}$), as well as Beier *Pkd1* heterozygous mice (*Pkd1*$^{m1Bei/flox}$) and *Oc*-Cre negative control mice (*Pkd1*$^{flox/+}$, equivalent to wild-type). These mice were used for phenotypic analysis. Animal experiments were performed following review and approval by University of Kansas Medical Center's Animal Care and Use Committee.

Genotyping PCR and real-time PCR to detect mutations and deletions — Genomic DNA was prepared from bone and other tissue specimens using standard procedures. PCR genotyping was performed using the following primers (19) (Fig 1A): F1, 5'-CTT CTA TCG CCT TCT TGA CGA GTT C-3'; R1, 5'-AGG GCT TTT CTT GCT GGT CT-3'; R2, 5'-TCG TGT TCC CTT ACC AAC CCT C-3'. *Pkd1* floxed (*Pkd1*^{flox}) alleles were identified in 2% agarose gels as 670-bp bands (Fig 1B). The delta floxed *Pkd1* (*Pkd1*$^{\Delta flox}$) allele was detected as a 0.85-kb band in 1% agarose gels (Fig 1B). The *Pkd1*^{m1Bei} allele was genotyped using SYBR® Green (Bio-Rad) real-time PCR as previously described (18).

Bone Densitometry, histomorphometric and Micro-CT analysis — Bone mineral density (BMD) of femurs was assessed at 16 weeks of age using a LUNAR$_{PIXIMUS}$ bone densitometer (Lunar Corp, Madison, WI). Calcein (Sigma, St. Louise, MO) double labeling of bone and histomorphometric analyses of periosteal mineral apposition rate (MAR), mineralized surface per bone surface (MS/BS), and bone formation rate (BFR) in tibias were performed using the osteomeasure analysis system (Osteometrics). Goldner and Von Kossa staining were performed according to standard protocols (21,22). The distal femoral metaphyses were also scanned using a Scanco μCT 40 (Scanco Medical AG, Brüttisellen, Switzerland). A 3D images analysis was done to determine bone volume (BV/TV) and cortical thickness (Ct.Th) as previously described (18,21).

Detection of bone marrow adipocytes in long bones by oil red O lipid staining — Whole intact femurs with encapsulated marrow were dissected from 18 weeks old mice, fixed for 48 hours in phosphate buffered paraformaldehyde, decalcified in 14% EDTA and then embedded in tissue freezing medium. Cryosectioning was performed on a Leica CM1900 Cryostat (Leica, Nussloch, Germany) equipped with a CryoJane frozen sectioning kit (Instrumedics, Hackensack, NJ). 10 μm thick sections were then stained with oil red O (ORO) for bone marrow adipocytes as described before (23). Briefly, the sections were rinsed in 60% isopropanol, stained for 20 minutes in 0.5% ORO-isopropanol solution, differentiated in 60% isopropanol, rinsed in tap water and mounted in glycerin jelly. Sections were examined with a Leica DM LB microscope equipped with an Optronics digital camera.

Detection of bone marrow fat in long bones by Micro-CT — Whole intact tibiae with encapsulated marrow were dissected from 18 weeks old mice, fixed for 48 hours in phosphate buffered paraformaldehyde, decalcified in 14% EDTA and stained for 2 hours in 2% aqueous osmium tetroxide (OsO_4). Bones were rinsed in water for 48 hours and then scanned at 6 μm resolution using a Scanco μCT40, 45 KeVp and 177 μA. Quantification of fat volume, density, and distribution throughout the marrow was registered to low contrast decalcified bone.

Real-time RT-PCR — For quantitative real-time RT–PCR, 2.0 μg total RNA isolated from either the long bone of 16-week-old mice or 10-days cultured primary osteoblasts in differentiation media was reverse transcribed as previously described (24). PCR reactions contained 100 ηg template (cDNA or RNA), 300 ηM each forward and reverse primers, and 1X iQ^{TM} SYBR$^{®}$ Green Supermix (Bio-Rad, Hercules, CA) in 50 μl. The threshold cycle (Ct) of tested-gene product from the indicated genotype was normalized to the Ct for cyclophilin A. Expression of total *Pkd1* transcripts was performed using the following *Pkd1*-allele-specific primers: In exon 26, forward primer of normal *Pkd1*$^{+}$ transcript: 5'- CTG GTG ACC TAT GTG GTC AT -3', forward primer of mutant *Pkd1*^{m1Bei} transcript: 5' - CTG GTG ACC TAT GTG GTC AG -3', and common reverse primer: 5' - AGC CGG TCT TAA CAA GTA TTT C -3'. In exon 2-4, forward primer of normal *Pkd1*$^{+}$ transcript: 5' - ATA GGG CTC CTG GTG AAC CT -3' and reverse primer: 5' - CCA CAG TTG CAC TCA AAT GG -3'. The normal *Pkd1*$^{+}$ vs cyclophilin A is normalized to the mean ratio of 5 control mice, which has been set to 1. The percentage of conditional deleted and mutant transcripts was calculated from the relative levels of the normal *Pkd1*$^{+}$ transcripts in different *Pkd1* exons (25).

Serum Biochemistry—Serum osteocalcin levels were measured using a mouse osteocalcin EIA kit (Biomedical Technologies Inc. Stoughton, MA, USA). Serum urea nitrogen (BUN) was determined using a BUN diagnostic kit from Pointe Scientific, Inc. Serum calcium (Ca) was measured by the colorimetric cresolphthalein binding method, and phosphorus (P) was measured by the phosphomolybdate–ascorbic acid method (Stanbio Laboratory, TX, USA). Serum TRAP was assayed with the ELISA-based SBA Sciences mouseTRAP^{TM} assay (Immunodiagnostic Systems, Fountain Hills, AZ).

Primary osteoblast culture for proliferation, differentiation, and western blot analysis — Primary osteoblasts from newborn mouse calvarias were cultured in α-MEM containing 10% FBS and 1% P/S as previously described (24). Cell proliferation was detected by BrdU incorporation assays as the manufacturer describes (QIA58, Calbiochem, Gibbstown, NJ). To induce differentiation, primary osteoblasts were plated at a density of 1x 10^{5} cells per well in a 6-well plate, and grown for period of up to 21 days in α-MEM containing 10% FBS supplemented with 5 mM β-glyceropho-phate and 25 μg/ml of ascorbic acid. Alkaline phosphatase activity and Alizarin red-S histochemical staining for mineralization were performed as previously described (24). Total DNA content was measured with a PicoGreen$^{®}$ dsDNA quantitation reagent and kit (Molecular Probes, Eugene, OR).

To examine the amounts of cytoplasmic Akt, Gsk, and β-catenin, the cells were prepared using 1x Passive Lysis Buffer for 30 minutes at 4 °C (Promega, Madison, WI) and centrifuged at 100,000g for 45 minutes at 4 °C. Protein concentrations of the supernatant were determined with a Bio-Rad protein assay kit (Bio-Rad, Hercules, CA). Equal quantities of protein were subjected to Nu-PAGE^{TM} 4-12% Bis-Tris Gel (Invitrogen, Carlsbad, CA) and were analyzed with standard Western blot protocols (HRP-conjugated secondary antibodies from Santa Cruz Biotechnology and ECL from Amersham Biosciences, Buckinghamshire, UK). Antibodies against phospho-Akt (ser-473), Akt, phospho-GSK (ser9), GSK were from Cell Signaling Technology (Beverly, MA). Anti-β-catenin (sc-7199) and Anti-β-actin (sc-47778) antibodies were from Santa Cruz Biotechnology.

Transient transfection — Both MC3T3-E1 and primary osteoblasts were cultured in α-MEM containing 10% fetal bovine serum (FBS) and 1% penicillin/streptomycin (P/S). To examine if PC1 regulates *Runx2*-P1 promoter activity by coupling with PI3K-Akt signaling, a number of 1 x 10^{6} of MC3T3-E1 cells were transfected with either control expression vector (sIg∅) or gain-of-function PC1 C-tail construct (PC1-AT) along with the *Runx2*-P1 luciferase reporter (p0.42*Runx2*-P1-Luc) construct by electroporation using Cell Line Nucleofector Kit R according to the manufacturer's protocol (Amaxa Inc, Gaithersburg, MD). A total of 10.2 μg of plasmid DNA was used for each electroporation, with 3.6 μg of PC1 C-tail construct, 2.4 μg of p0.42*Runx2*-P1-Luc reporter, the indicated amounts of a dominant-negative *Akt* (dn-*Akt*) construct in combination with empty vector (3.6 μg), and 0.6 μg of Renilla luciferase-null (RL-null) as internal control plasmid. Promoter activity was assessed by measuring luciferase activity 48 hours after transfection in the presence or absence of a PI3K inhibitor (0.1~10 μM, LY294002) and a dn-*Akt* construct (1.2~3.6 μg) as previously described (17,18).

To explore potential abnormalities of the Wnt pathway in excised floxed *Pkd1* null mice, control (*Pkd1*$^{flox/+}$) and excised floxed *Pkd1* null (*Pkd1*$^{Oc\text{-}cko}$) osteoblasts were transiently cotransfected with either pTOPFLASH or pFOPFLASH along with *Renilla* luciferase-null (RL-null, Promega, Madison, WI) as an internal control as described above. Promoter activity will be assessed by measuring luciferase activity 48 hours after transfection in the presence or absence of 100 ng/ml of recombinant Wnt3a treatment for last 8 hours.

Statistics — We evaluated differences between groups by one-way analysis of variance. All values are expressed as means ± S.D. All computations were performed using the GraphPad Prism5 (GraphPad Software Inc. La Jolla, CA).

RESULTS

Oc-Cre mediated bone-specific deletion of Pkd1 —The four genotypes from the breeding strategy (*Oc*-Cre;*Pkd1*$^{\text{flox/m1Bei}}$ or *Pkd1*$^{\text{Oc-cKO}}$, *Oc*-Cre;*Pkd1*$^{\text{flox/+}}$, *Pkd1*$^{\text{flox/m1Bei}}$, and *Pkd1*$^{\text{flox/+}}$) were born at the expected Mendelian frequency and all exhibited survival indistinguishable from wild-type mice. The normal survival of conditional *Pkd1*$^{\text{Oc-cKO}}$ null mice (*Oc*-Cre;*Pkd1*$^{\text{flox/m1Bei}}$) contrasts with perinatal lethality of homozygous *Pkd1*$^{\text{m1Bei/m1Bei}}$ mice (17). *Oc*-Cre expression is limited to cells of the osteoblast lineage (late osteoblasts>osteocytes) with onset of expression just before birth and persisting throughout the mature osteoblast lineage (20). To confirm that the *Pkd1* floxed allele was selectively deleted in bone, we performed PCR analysis using a combination of primers that specifically detect floxed *Pkd1* alleles (*Pkd1*$^{\text{flox}}$) and the excised floxed *Pkd1* alleles (*Pkd1*$^{\Delta\text{flox}}$) in *Oc*-Cre;*Pkd1*$^{\text{flox/+}}$ or *Oc*-Cre;*Pkd1*$^{\text{flox/m1Bei}}$ mice, (Fig. 1A). We demonstrated that *Oc*-Cre-mediated floxed recombination occurred exclusively in tissues that contain osteoblastic cells, whereas non-skeletal tissues retained the intact floxed *Pkd1* alleles (*Pkd1*$^{\text{flox}}$) (Fig. 1B). The *Pkd1*$^{\text{m1Bei}}$ mutation, which functions as a null allele, was used in combination with the floxed *Pkd1* allele (*Pkd1*$^{\text{flox}}$) to increase the net efficiency of *Pkd1* inactivation by Cre-recombinase to reduce functional *Pkd1* expression. Therefore, we examined the percentage of *Pkd1* conditional deleted and the *Pkd1*$^{\text{m1Bei}}$ mutant alleles in bone. The level of conditional deleted *Pkd1*$^{\Delta\text{flox}}$ alleles and the presence of the *Pkd1*$^{\text{m1Bei}}$ mutation from the femurs of these four genotypes mice were assessed by real time PCR (Fig. 1C). Both *Pkd1*$^{\text{flox/m1Bei}}$ and *Oc*-Cre; *Pkd1*$^{\text{flox/m1Bei}}$ mice expressed 50% percent of *Pkd1*$^{\text{m1Bei}}$ mutant allele, whereas *Oc*-Cre;*Pkd1*$^{\text{flox/+}}$ and *Oc*-Cre;*Pkd1*$^{\text{flox/m1Bei}}$ mice exhibited approximately 25% excision of the floxed Exon 2-4 from *Pkd1*, indicating that *Oc*-Cre mediated bone-specific deletion of the floxed *Pkd1* allele *is* incomplete (Fig. 1C). The combined effect *Pkd1*$^{\text{m1Bei}}$ and (*Pkd1*$^{\Delta\text{flox}}$) in *Oc*-Cre; *Pkd1*$^{\text{flox/m1Bei}}$ resulted in a net reduction of Pkd1 expression by ~75% in bone (Fig 1C). Real time RT-PCR to assess the level of expression of the residual functional *Pkd1* transcript confirmed the progressive reduction of functional *Pkd1* message in conditional mutant mice, *i.e.*, *Pkd1*$^{\text{flox/+}}$ (100%), *Oc*-Cre;*Pkd1*$^{\text{flox/+}}$ (76%), *Pkd1*$^{\text{flox/m1Bei}}$ (50%), and *Oc*-Cre; *Pkd1*$^{\text{flox/m1Bei}}$ (25%) mice (data not shown). In addition, *Oc*-Cre;*Pkd1*$^{\text{flox/m1Bei}}$ mice heterozygous for the conditional deleted *Pkd1*$^{\Delta\text{flox}}$ allele and mutant *Pkd1*$^{\text{m1Bei}}$ allele demonstrated no cyst formation in the kidney, consistent with the bone specific inactivation of *Pkd1* (Fig 1D). In contrast, positive control mice lacking Pkd1 in the kidney have massive cyst formation in the kidney (Fig 1D).

Additive effects of global mutant (Pkd1$^{\text{m1Bei}}$*) and conditional deleted (Pkd1*$^{\Delta\text{flox}}$*) Pkd1 alleles suggests a direct role for Pkd1 in bone* —At 16-weeks of age, the gross appearance and body weight of single global and conditional heterozygous (*Pkd1*$^{\text{flox/m1Bei}}$ or *Oc*-Cre;*Pkd1*$^{\text{flox/+}}$) and control (*Pkd1*$^{\text{flox/+}}$) mice were not significantly different. The global *Pkd1* heterozygous mice (*Pkd1*$^{\text{flox/m1Bei}}$) and heterozygous conditional deleted *Pkd1* mice (*Oc*-Cre;*Pkd1*$^{\text{flox/+}}$), however, were osteopenic, as evidenced by respective 9% and 7% reduction BMD in both male and female adult mice (Fig. 2A). The phenotype of the *Pkd1*$^{\text{Oc-cKO}}$ mice was more severe. The body weight of both male and female *Pkd1*$^{\text{Oc-cKO}}$ mice was reduced by approximately 16% and 12% (data not shown) compared to the control mice (*Pkd1*$^{\text{flox/+}}$). In addition, *Pkd1*$^{\text{Oc-cKO}}$ mice had greater loss in BMD, with respective reductions in BMD of 14% and 13% reduction in male and female adult mice (Fig. 2A). The abnormalities in BMD in the various groups, though present at 6 weeks of age, segregated by gene-dose by 16 weeks of age (Fig 2B).

μCT analysis revealed that the reduction in bone mass in heterozygous *Pkd1* deficient mice (either *Pkd1*$^{\text{flox/m1Bei}}$ or *Oc*-Cre;*Pkd1*$^{\text{flox/+}}$) was caused by a reduction in trabecular bone volume (24.3% and 25.5%, respectively) and cortical bone thickness (9.7% and 10.8%, respectively) (Fig. 2C). *Pkd1*$^{\text{cKO/m1Bei}}$ had greater loss in both trabecular (44.5%) and cortical bone (21.0%) than did single heterozygous mice (Fig. 2C).

Consistent with a low-bone-mass phenotype by BMD and μCT analysis, both Goldner staining in distal femur and Von Kossa staining in vertebrae confirmed marked reductions in bone volume and cortical thickness in *Pkd1*$^{\text{Oc-cKO}}$ null mice (Fig. 3A). In addition, we found that bone loss was associated with a significant *Pkd1* gene dose-dependent decrease in periosteal mineral apposition rate (MAR), mineralized surface per bone surface (MS/BS), and bone formation rate (BFR). In this regard, MAR, MS/BS, and BFR were reduced by ~36%, ~33%, and ~57% in heterozygous *Pkd1*$^{\text{flox/m1Bei}}$ and *Oc*-Cre;*Pkd1*$^{\text{flox/+}}$ mice and ~65%, ~60%, and ~87% in *Pkd1*$^{\text{Oc-cKO}}$ null mice compared with age-matched controls, respectively (Fig. 3B).

To investigate the effects of *Pkd1* deficiency on gene expression profiles in bone, we examined by real-time RT-PCR the expression levels of a panel of osteoblast lineage-, osteoclast-, and chondrocyte-related mRNAs from the femurs of 16-week-old control, heterozygous *Pkd1* deficient (*Oc*-Cre;*Pkd1*$^{\text{flox/+}}$ and *Pkd1*$^{\text{m1Bei/+}}$), and *Oc*-Cre;*Pkd1*$^{\text{flox/m1Bei}}$ mice (Table I). Bone derived from heterozygous *Oc*-Cre;*Pkd1*$^{\text{flox/+}}$ and *Pkd1*$^{\text{m1Bei/+}}$ mice had measurable reductions in the osteoblast-lineage gene transcripts, including *Runx2*-II, total *Runx2*, *Osteocalcin, Osteopontin, Bsp, Osteoprotegerin (Opg), Rank ligand (RankL)*, *Dmp1*, and *Phex* mRNA levels compared to control mice. Significantly greater reductions of *Runx2*-II, total *Runx2*, *Osteocalcin, Osteopontin, Bsp, RankL, and Dmp1* were observed in *Pkd1*$^{\text{Oc-cKO}}$ null mice. In this regard, the *Opg/RankL* expression ratio was increased in a gene dose-dependent manner (Table I). Consistent with a ratio of Opg/*RankL* that favors the reduced osteoclastogenesis, bone expression of *Trap* and *Mmp9*, markers of bone resorption, were also reduced in heterozygous *Pkd1* deficient mice and to a greater extent in *Pkd1*$^{\text{Oc-cKO}}$ null mice (Table I). Transcripts of chondrocyte-related genes did not differ between heterozygous *Pkd1* deficient and *Pkd1*$^{\text{Oc-cKO}}$ null mice (Table I).

Changes in gene expression in bone correlated with alterations in serum biomarkers. In this regard, further evidence for osteoblast dysfunction includes a reduction in *Osteocalcin* in serum from 16-week-old heterozygous *Oc*-Cre;*Pkd1*$^{\text{flox/+}}$ and *Pkd1*$^{\text{m1Bei/+}}$ mice (Table II). Serum levels of TRAP, a marker of bone resorption, were also reduced in heterozygous *Pkd1*-deficient mice compared to control littermates (Table II). As with other parameters, *Pkd1*$^{\text{Oc-cKO}}$ null mice had greater reductions in bone formation and resorption markers, indicating additive effects of inactivation of both *Pkd1* alleles in bone homeostasis. Collectively, these findings suggest that *Pkd1*-mediated bone loss results from low bone formation rates rather than increased bone resorption (Fig. 2, A-C, Table II).

PPARγ, an adipocyte transcription factor, and adipocyte markers, including lipoprotein lipase (*Lpl*) and adipocyte fatty acid-binding protein 2 (*aP*2) were increased femurs of *Pkd1* deficient mice in a *Pkd1* gene dosage-related manner (Table I). Consistent with increased adipogenic markers, bone marrow exhibited an increased percentage of fat cells in *Pkd1*$^{\text{Oc-cKO}}$ mice, as evidenced by a higher number of adipocytes and volume of fat droplets in decalcified femurs and tibias stained with Oil Red O and Osmium tetroxide (OsO4) (Fig 3C). In addition, the inflammatory cytokine *IFNγ*, but not *TNFα* and *TRAIL* expression levels, was significantly elevated in *Pkd1* deficient mice (Table I). Moreover, *Alox15*, arachidonate 15-lipoxygenase, was also markedly increased in conditional *Pkd1* deficitn mice.

Effect of conditional deletion Pkd1 on osteoblastic function ex vivo — To determine the impact of conditional deleted *Pkd1* on osteoblast function *ex vivo*, we examined cell proliferation and osteoblastic differentiation and gene expression profiles in primary osteoblast cultures derived from control and *Pkd1*$^{\text{Oc-cKO}}$ null mice. Consistent with defects in bone formation, we found that *Pkd1*$^{\text{Oc-cKO}}$ null osteoblasts had a higher BrdU incorporation than control osteoblasts, indicating a greater proliferation rate in *Pkd1*$^{\text{Oc-cKO}}$ null osteoblasts (Fig. 4A). In addition, conditional null osteoblasts displayed impaired osteoblastic differentiation and maturation, as evidenced by lower alkaline phosphatase activity, diminished calcium deposition in extracellular matrix, and reduced osteoblastic differentiation markers compared to controls (Fig. 4B-4D). In agreement with increased adipogenic activity *in vivo*, the cultured primary calvarial cells under osteogenic condition exhibited a markedly increase of adipocyte markers, including *PPARγ*, *aP2*, and *Lpl* (Fig. 4E), suggesting impairment of osteogenesis and enhancement of adipogenesis in *Pkd1*$^{\text{Oc-cKO}}$ null osteoblast cultures.

Effect of conditional deletion Pkd1 on PI3K-Akt-Gsk-β-catenin signaling pathway in osteoblasts. PC1 encoded by *Pkd1* is coupled to multiple signal transduction pathways, including activation of canonical Wnt/ β–catenin and Akt-dependent pathways. There is evidence Akt-dependent serine 9 phosphorylation of GSK-3β that prevents phosphorylation and degradation of β-catenin (26-29). Because the phosphatidylinositol 2-kinase (PI3-kinase)/Akt pathway and Wnt signaling play a role in osteoblastic development (30,31), we determined the level of Akt phosphorylation in *Pkd1*$^{\text{Oc-cKO}}$ derived osteoblasts. Basal phospho-Akt relative to total Akt expression and phosphorylation of serine 9 of GSK-3β were reduced in *Pkd1*$^{\text{Oc-cKO}}$ null osteoblasts compared to controls. To determine if potential cross-talk between PC1/PI3K/Akt pathway and the Wnt/GSK3β/β–catenin pathways have functional consequences (28), we next examined the response of osteoblasts derived from *Pkd1*$^{\text{Oc-cKO}}$ mice to Wnt3a. *Pkd1*$^{\text{Oc-cKO}}$ derived osteoblasts had a reduced response to Wnt3a-mediated phosphorylation of Akt when compared to control cells (Fig. 5A). In contrast, addition of Wnt3a resulted in an increase in phosphorylation of GSK3β in control cells, leading to the inactivation of GSK3β (Fig. 5A). To determine if inhibition of GSK3β activated β-catenin (32), we assessed the accumulation of free β-catenin in the cytoplasm (33). Consistent with reduction of GSK3β phosphorylation, we found that the basal level of cytosolic β-catenin was lower in *Pkd1*$^{\text{Oc-cKO}}$ null osteoblasts and exhibited no increase following Wnt3a treatment, whereas control cells increased cytoplasmic β-catenin levels following Wnt3a stimulation (Fig. 5A).

To examine the effect of Pkd1 inactivation on Wnt/β-catenin transcriptional activity, we examined TOPFlash activity in *Pkd1*$^{\text{Oc-cKO}}$ null osteoblasts. We observed a significant reduction of basal TOPFLASH activity in primary osteoblasts derived from *Pkd1*$^{\text{Oc-cko}}$ mice compared to the controls. In addition, Wnt3a-induced TOPFLASH activity was more than 2-fold above basal level in the control osteoblasts, whereas Wnt3a induced TOPFLASH activity was only 1.4-fold above basal level in the *Pkd1*$^{\text{Oc-cKO}}$ null mice (Fig. 5B), indicating loss of PC1 significantly attenuates responsiveness of the Wnt/β-catenin pathway in osteoblasts.

To examine the role of PC1-dependent Akt activation on transcriptional control of osteoblasts development, we examined *Runx2*-II promoter activity. In previous studies we have shown that PC1 is coupled to *Runx2-II* expression, a master regulator in osteoblast function, and that transfection of the C-terminal region of PC1 (PC1-AT) was sufficient to activate the *Runx2*-II P1 promoter/reporter construct (17). As shown in Fig. 5C and 5D, we found that either the PI3K inhibitor LY294002 or cotransfection with a dominant negative Akt (dn-Akt) construct resulted in a dose-dependent inhibition of PC1-AT-mediated increase in *Runx2*-II P1 promoter activity.

Examination of Wnt-related gene expression in *Pkd1*$^{\text{Oc-cKO}}$ null osteoblasts further supports impairment of Wnt/β-catenin signaling. In this regard, we found evidenced for down-regulation of *Wnt10b*, *Axin2*, *Cox2* and *Runx2*-II, and up-regulation of the negative regulators *sFrp1* and *sFrp4* (Fig. 5E).

DISCUSSION

PC1 is expressed in cells within the osteoblast lineage (18), and skeletal abnormalities have been reported in *Pkd1* mutant mouse models (14,15,17,18), but from these generalized loss-of-function observations it was not clear if the observed skeletal abnormalities were an indirect consequence of loss of PC1 in multiple tissues or a direct effect of loss of PC1 in osteoblasts. In the present studies, we have addressed this question by using *Oc*-Cre to conditionally inactivate *Pkd1* in mature osteoblasts postnatally. First, we have shown that the heterozygous conditional reduction of *Pkd1* in osteoblasts in *Oc*-Cre;*Pkd1*$^{\text{flox/+}}$ results in an osteopenic bone phenotype indistinguishable from the global *Pkd1*$^{\text{flox/m1Bei}}$ mice. Since *Oc*-Cre;*Pkd1*$^{\text{flox/+}}$ mice had ~25% reduction in *Pkd1* expression, whereas *Pkd1*$^{\text{flox/m1Bei}}$ mice had a 50% reduction, but had identical effects on bone, suggest that loss of Pkd1 function in osteoblasts is responsible for the observed reduction in bone mass in both models. Moreover, the additive effects on the severity of osteopenia in combined conditional deletion of *Pkd1* in osteoblasts superimposed on the inactivated *Pkd1*$^{\text{m1Bei}}$ allele in *Oc*-Cre;*Pkd1*$^{\text{flox/m1Bei}}$ (or *Pkd1*$^{\text{Oc-cKO}}$) mice, which resulted in approximately 2-fold greater (~ 14%) reduction in BMD associated with a 75% overall reduction in *Pkd1* expression in bone, compared to a 50% reduction in other tissues, indicates a dose-dependent function of *Pkd1* in mature osteoblasts.

We purposely did not create *Oc*-Cre; *Pkd1*$^{\text{flox/flox}}$ mice, due to the relative inefficiency of the *Oc*-Cre, which based on the 25% reduction in

Pkd1 transcripts observed in *Oc*-Cre;*Pkd1*$^{flox/+}$ mice may have only reduced expression in *Oc*-Cre; *Pkd1*$^{flox/flox}$ mice to levels similar to the heterozygous *Pkd1*$^{flox/m1Bei}$ mice (e.g., 50%). So, to achieve greater reduction in *Pkd1* expression in osteoblasts (*e.g.*, ~75%), we created *Oc*-Cre; *Pkd1*$^{flox/m1Bei}$ mice. It is of note that the magnitude of bone loss in *Pkd1*$^{Oc-cKO}$ mice is comparable to the 16% reduction in BMD found in Lrp5 null mice (34), a receptor known to have important anabolic osteoblast-mediated functions in bone through activation of canonical Wnt signaling pathways and exceeds bone loss observed in oophorectomized mice (which is typically <10%) (35). Since *Pkd1*$^{Oc-cKO}$ had no demonstrable extraskeletal phenotypes and loss of *Pkd1* was greatest in bone, these findings are most consistent with a direct role of PC1 to regulate osteoblast function. Evidence for impaired osteoblastic function in *Pkd1*$^{Oc-cko}$ null mice is evident from both *in vivo* and *ex vivo* analysis. Bone from *Pkd1*$^{Oc-cko}$ null mice displayed decreased MAR, MS/BS, BFR, and reduced expression of osteoblastic markers, including the *Runx2*-II isoform, which regulates osteoblast development and function.

Ex vivo assessment of primary osteoblasts isolated confirmed an intrinsic impairment of osteoblast maturation as well as identified increased proliferation, which are typically inversely related (36). A feature of ADPKD renal cells is increased proliferation rate as well as impaired differentiation of epithelial cells (37); our findings suggest that this phenotypic switch may also occur in osteoblasts. Indeed, the *Pkd1*$^{Oc-cKO}$ null osteoblasts showed a greater proliferation rate as well as impaired osteoblastic differentiation and maturation. Since others have shown that the response of the renal epithelium to acquired loss of *Pkd1* is determined by the developmental state of the organ (38), our data showing a defect in osteoblast maturation in remodeling bone raises the possibility that *Pkd1* may also play a role in the embryogenesis of bone. Osteoblasts and adipocytes undergo renewal from bone marrow derived precursors and ratio of osteoblasts and adipocytes appear to be reciprocally controlled in response to physiological stimuli and aging (39). We also found an inverse dose relationship between *Pkd1* expression and adipogenesis marker expression in the *Pkd1*$^{Oc-cKO}$ osteoblast cultures compared to the control. In agreement with this *in vitro* data, our *in vivo* study also showed strong evidence for lipid droplet accumulation in the bone marrow of *Pkd1*$^{Oc-cKO}$ mice compared with the control mice via Oil Red O and Osmium staining. This phenomenon was also supported an enhanced expression of inflammatory mediators such as *IFNγ* and *Alox15* (40,41), which produced by adipose tissues strongly suppress osteoblastogenesis. The findings of increased fat cells in bone marrow of *Pkd1*$^{Oc-cKO}$ mice and impaired development of osteoblast cultures derived from *Pkd1*$^{Oc-cKO}$ mice suggest that Pkd1 deficiency may lead to impaired differentiation of mesenchymal stem cells into osteoblasts and enhanced differentiation into adipocytes.

Since *Oc*-Cre mediated deletion of *Pkd1* in osteoblasts would carry forward to the terminal differentiated osteocytes, we cannot exclude a possible role of the osteocyte in the bone phenotype in *Pkd1*$^{Oc-cko}$ null mice. In addition to being expressed throughout the osteoblastic lineage during embryogenesis and in postnatal bone, *Pkd1* is also expressed in chondrocytes (6). Consequently, the more severe skeletal abnormalities in global *Pkd1* null compared to *Pkd1*$^{Oc-cKO}$ mice could be due to PC1 regulation of osteoblast differentiation or chondrocyte function during development or to systemic effects caused by the presence of polycystic kidneys (6,7). Additional studies that ablate *Pkd1* in earlier in the osteoblast lineage during embryogenesis or later in osteocytes, as well in mature and immature chondrocytes, will be needed to establish a direct role of PC1 in skeletal development and to establish the respective contributions of *Pkd1* function in pre-osteoblasts, osteoblasts, osteocytes and chondrocytes.

We previously demonstrated that PC1 selectively regulates *Runx2*-II P1 promoter activity in osteoblasts through an intracellular calcium pathway linked to nuclear factor I family and AP-1 transcription factors (17). The PC1 regulates a variety of signal transduction pathways in renal epithelial cells, including Akt1 and GSK3β (26-28), which are also important regulators of bone mass (42,43). The present studies indicate that Pkd1 also regulates PI3K-Akt-GSK3β signaling in osteoblasts, and that this pathway is upstream of Runx2. The decline in Akt-GSK3β-β-catenin signaling in osteoblasts from *Pkd1*$^{Oc-cko}$ null mice and the finding that PC1-PI3K-Akt signaling regulates *Runx2*-II P1 promoter activity, suggests that this may represent another *Pkd1*-dependent pathway regulating osteoblasts function. The interactions between Wnt and Pkd1 dependent signaling pathways, however, are complex, and further studies will be needed to define the mechanism whereby loss of polycystin 1 results in decreased β-catenin activity.

The broader role of PC1 in regulating bone physiology is not revealed by our studies. There is no known ligand for PC. Polycystin potentially functions as a mechanosensor, a chemosensor, or as a sensor of cell-cell or cell-matrix interactions (44,45). PC1 colocalizes to the primary cilium (46), which is also present in osteoblasts, osteocytes and chondrocytes (47,48). Also cleavage of PC1 at the G protein- coupled receptor proteolytic site (GPS) upstream of the first TM segment may be required for bioactivity (49), suggesting that PC1 may be constitutively active. Although the precise activator in bone remains to be defined, PC1 presence or its ability to sense environmental cues during bone remodeling may allow it to function as a "hub" or a common connection point that permits cells in the osteoblast lineage to sense diverse environmental signals during skeletal development and translate these into multiple signaling pathways required for maintenance of bone mass.

In contrast to the role of *Pkd1* in mouse bone, a PC1-dependent bone phenotype has not been reported in humans with ADPKD, who have superimposed renal osteodystrophy. It may yet be possible to detect small, clinically unapparent reductions of bone density in humans heterozygous for *PKD1* mutations prior to developing kidney failure. In addition, there are some very interesting but rare families with early onset of polycystic kidney disease in newborns that are associated with severe skeletal malformations, similar to those observed in mice with homozygous *Pkd1* mutations, suggesting that broadly disrupting both alleles in osteoblasts /osteocytes (analogous to the *Pkd1* null mouse as opposed to random second hits in ADPKD) might cause clinically apparent bone disease in humans (12,50).

In conclusion, the finding that selective reduction of *Pkd1* in osteoblasts results in osteopenia defines a new signaling paradigm in bone that has the potential expand our understanding of how bone senses environmental signals maintaining bone mass as well as regulating osteoblast growth and development. The further study of polycystin function in bone could provide a variety of new insights, ranging from new mechanosensing mechanisms potentially involving primary cilium to identifying a moleuclar target for the development of pharmacological approaches to increased bone mass in osteopenic disorders.

REFERENCES

1. Xu, H., Shen, J., Walker, C. L., and Kleymenova, E. (2001) *DNA Seq* **12**, 361-366
2. Chauvet, V., Qian, F., Boute, N., Cai, Y., Phakdeekitacharoen, B., Onuchic, L. F., Attie-Bitach, T., Guicharnaud, L., Devuyst, O., Germino, G. G., and Gubler, M. C. (2002) *Am J Pathol* **160**, 973-983
3. Wilson, P. D. (2004) *N Engl J Med* **350**, 151-164
4. Gabow, P. A. (1993) *N Engl J Med* **329**, 332-342
5. Torra, R., Badenas, C., San Millan, J. L., Perez-Oller, L., Estivill, X., and Darnell, A. (1999) *Am J Hum Genet* **65**, 345-352
6. Lu, W., Shen, X., Pavlova, A., Lakkis, M., Ward, C. J., Pritchard, L., Harris, P. C., Genest, D. R., Perez-Atayde, A. R., and Zhou, J. (2001) *Hum Mol Genet* **10**, 2385-2396
7. Boulter, C., Mulroy, S., Webb, S., Fleming, S., Brindle, K., and Sandford, R. (2001) *Proc Natl Acad Sci U S A* **98**, 12174-12179
8. Peczkowska, M., Januszewicz, A., Grzeszczak, W., Moczulski, D., Janaszek-Sitkowska, H., Kabat, M., Biederman, A., Hendzel, P., Prejbisz, A., Cendrowska-Demkow, I., Zielinski, T., and Januszewicz, M. (2004) *Blood Press* **13**, 283-286
9. van Dijk, M. A., Chang, P. C., Peters, D. J., and Breuning, M. H. (1995) *J Am Soc Nephrol* **6**, 1670-1673
10. Hassane, S., Claij, N., Lantinga-van Leeuwen, I. S., Van Munsteren, J. C., Van Lent, N., Hanemaaijer, R., Breuning, M. H., Peters, D. J., and DeRuiter, M. C. (2007) *Arterioscler Thromb Vasc Biol* **27**, 2177-2183
11. Housset, C. (2005) *Gastroenterol Clin Biol* **29**, 861-869
12. Watnick, T. J., Torres, V. E., Gandolph, M. A., Qian, F., Onuchic, L. F., Klinger, K. W., Landes, G., and Germino, G. G. (1998) *Mol Cell* **2**, 247-251
13. Driscoll, J. A., Bhalla, S., Liapis, H., Ibricevic, A., and Brody, S. L. (2008) *Chest* **133**, 1181-1188
14. Kolpakova-Hart, E., McBratney-Owen, B., Hou, B., Fukai, N., Nicolae, C., Zhou, J., and Olsen, B. R. (2008) *Dev Biol* **321**, 407-419
15. Kolpakova-Hart, E., Nicolae, C., Zhou, J., and Olsen, B. R. (2008) *Matrix Biol* **27**, 505-512
16. Hou, B., Kolpakova-Hart, E., Fukai, N., Wu, K., and Olsen, B. R. (2009) *Bone* **44**, 1121-1133
17. Xiao, Z., Zhang, S., Magenheimer, B. S., Luo, J., and Quarles, L. D. (2008) *J Biol Chem* **283**, 12624-12634
18. Xiao, Z., Zhang, S., Mahlios, J., Zhou, G., Magenheimer, B. S., Guo, D., Dallas, S. L., Maser, R., Calvet, J. P., Bonewald, L., and Quarles, L. D. (2006) *J Biol Chem* **281**, 30884-30895
19. Piontek, K. B., Huso, D. L., Grinberg, A., Liu, L., Bedja, D., Zhao, H., Gabrielson, K., Qian, F., Mei, C., Westphal, H., and Germino, G. G. (2004) *J Am Soc Nephrol* **15**, 3035-3043
20. Zhang, M., Xuan, S., Bouxsein, M. L., von Stechow, D., Akeno, N., Faugere, M. C., Malluche, H., Zhao, G., Rosen, C. J., Efstratiadis, A., and Clemens, T. L. (2002) *J Biol Chem* **277**, 44005-44012
21. Xiao, Z., Awad, H. A., Liu, S., Mahlios, J., Zhang, S., Guilak, F., Mayo, M. S., and Quarles, L. D. (2005) *Dev Biol* **283**, 345-356
22. Glass, D. A., 2nd, Bialek, P., Ahn, J. D., Starbuck, M., Patel, M. S., Clevers, H., Taketo, M. M., Long, F., McMahon, A. P., Lang, R. A., and Karsenty, G. (2005) *Dev Cell* **8**, 751-764
23. David, V., Martin, A., Lafage-Proust, M. H., Malaval, L., Peyroche, S., Jones, D. B., Vico, L., and Guignandon, A. (2007) *Endocrinology* **148**, 2553-2562
24. Xiao, Z. S., Hjelmeland, A. B., and Quarles, L. D. (2004) *J Biol Chem* **279**, 20307-20313

25. Lantinga-van Leeuwen, I. S., Leonhard, W. N., van de Wal, A., Breuning, M. H., Verbeek, S., de Heer, E., and Peters, D. J. (2006) *Genesis* **44**, 225-232
26. Boca, M., D'Amato, L., Distefano, G., Polishchuk, R. S., Germino, G. G., and Boletta, A. (2007) *Mol Biol Cell* **18**, 4050-4061
27. Boca, M., Distefano, G., Qian, F., Bhunia, A. K., Germino, G. G., and Boletta, A. (2006) *J Am Soc Nephrol* **17**, 637-647
28. Kim, E., Arnould, T., Sellin, L. K., Benzing, T., Fan, M. J., Gruning, W., Sokol, S. Y., Drummond, I., and Walz, G. (1999) *J Biol Chem* **274**, 4947-4953
29. Raucci, A., Bellosta, P., Grassi, R., Basilico, C., and Mansukhani, A. (2008) *J Cell Physiol* **215**, 442-451
30. Westendorf, J. J., Kahler, R. A., and Schroeder, T. M. (2004) *Gene* **341**, 19-39
31. Mukherjee, A., and Rotwein, P. (2009) *J Cell Sci* **122**, 716-726
32. Aoki, K., and Taketo, M. M. (2008) *Methods Mol Biol* **468**, 307-331
33. Constantinou, T., Baumann, F., Lacher, M. D., Saurer, S., Friis, R., and Dharmarajan, A. (2008) *J Mol Signal* **3**, 10
34. Iwaniec, U. T., Wronski, T. J., Liu, J., Rivera, M. F., Arzaga, R. R., Hansen, G., and Brommage, R. (2007) *J Bone Miner Res* **22**, 394-402
35. Kim, D., Cho, S. W., Her, S. J., Yang, J. Y., Kim, S. W., Kim, S. Y., and Shin, C. S. (2006) *Stem Cells* **24**, 1798-1805
36. Lian, J. B., and Stein, G. S. (1995) *Iowa Orthop J* **15**, 118-140
37. Yamaguchi, T., Wallace, D. P., Magenheimer, B. S., Hempson, S. J., Grantham, J. J., and Calvet, J. P. (2004) *The Journal of biological chemistry* **279**, 40419-40430
38. Piontek, K., Menezes, L. F., Garcia-Gonzalez, M. A., Huso, D. L., and Germino, G. G. (2007) *Nat Med* **13**, 1490-1495
39. Nuttall, M. E., and Gimble, J. M. (2000) *Bone* **27**, 177-184
40. Rocha, V. Z., Folco, E. J., Sukhova, G., Shimizu, K., Gotsman, I., Vernon, A. H., and Libby, P. (2008) *Circ Res* **103**, 467-476
41. Klein, R. F., Allard, J., Avnur, Z., Nikolcheva, T., Rotstein, D., Carlos, A. S., Shea, M., Waters, R. V., Belknap, J. K., Peltz, G., and Orwoll, E. S. (2004) *Science* **303**, 229-232
42. Kawamura, N., Kugimiya, F., Oshima, Y., Ohba, S., Ikeda, T., Saito, T., Shinoda, Y., Kawasaki, Y., Ogata, N., Hoshi, K., Akiyama, T., Chen, W. S., Hay, N., Tobe, K., Kadowaki, T., Azuma, Y., Tanaka, S., Nakamura, K., Chung, U. I., and Kawaguchi, H. (2007) *PLoS One* **2**, e1058
43. Kugimiya, F., Kawaguchi, H., Ohba, S., Kawamura, N., Hirata, M., Chikuda, H., Azuma, Y., Woodgett, J. R., Nakamura, K., and Chung, U. I. (2007) *PLoS One* **2**, e837
44. Weimbs, T. (2007) *Am J Physiol Renal Physiol* **293**, F1423-1432
45. Wilson, P. D., Geng, L., Li, X., and Burrow, C. R. (1999) *Lab Invest* **79**, 1311-1323
46. Li, Q., Montalbetti, N., Wu, Y., Ramos, A., Raychowdhury, M. K., Chen, X. Z., and Cantiello, H. F. (2006) *The Journal of biological chemistry* **281**, 37566-37575
47. Jensen, C. G., Poole, C. A., McGlashan, S. R., Marko, M., Issa, Z. I., Vujcich, K. V., and Bowser, S. S. (2004) *Cell Biol Int* **28**, 101-110
48. Takaoki, M., Murakami, N., and Gyotoku, J. (2004) *Biol Sci Space* **18**, 181-182
49. Qian, F., Boletta, A., Bhunia, A. K., Xu, H., Liu, L., Ahrabi, A. K., Watnick, T. J., Zhou, F., and Germino, G. G. (2002) *Proc Natl Acad Sci U S A* **99**, 16981-16986
50. Turco, A. E., Padovani, E. M., Chiaffoni, G. P., Peissel, B., Rossetti, S., Marcolongo, A., Gammaro, L., Maschio, G., and Pignatti, P. F. (1993) *J Med Genet* **30**, 419-422

FOOTNOTES

*We are particularly grateful to Dr. Gregory Germino at Johns Hopkins University for providing the floxed *Pkd1* mice. This work was supported by the grant R01-AR049712 and R21-AR056794 from the National Institutes of Health.

The abbreviations used are: ADPKD, autosomal dominant polycystic kidney disease; PKD1 or Pkd1, polycystic kidney disease gene 1; PKD2 or Pkd2, polycystic kidney disease gene 2; PC1, polycystin 1; PC2, polycystin 2; Runx2, Runt-related transcription factor 2; BMD, bone mineral density; μCT, microcomputed tomography; BV/TV, bone volume/total volume; Ct.Th., cortical bone thickness. *Bsp, Bone sialoprotein*; *Opg*, *Osteoprotegerin*; *Phex*, Phosphate-regulating gene with homologies to Endopeptidases on the X chromosome*; Dmp1*, dentin matrix protein 1; *Trap,* tartrate resistant acid phosphatase; *Mmp*, matrix metalloproteinase; *VegfA*, vascular endothelial growth factor A; *PPARγ*, peroxisome proliferator-activated receptor γ; *Lpl*, lipoprotein lipase; *aP2*, adipocyte fatty acid-binding protein 2; *IFNγ*, interferon-gamma; *TNFα*, tumour necrosis factor-alpha; *TRAIL*, tumor necrosis factor (TNF)-related apoptosis-inducing ligand; *Alox15*, arachidonate 15-lipoxygenase.

FIGURE LEGENDS

FIG. 1. ***Osteocalcin*(*Oc*)-Cre-mediated bone specific deletion of *Pkd1* from the floxed *Pkd1* allele (*Pkd1*$^{\text{flox}}$).** A, Schematic illustration of wild-type (*Pkd1*$^{+}$), mutant (*Pkd1*$^{\text{m1Bei}}$), and floxed *Pkd1* allele before (*Pkd1*$^{\text{flox}}$) and after deletion (*Pkd1*$^{\Delta\text{flox}}$) of the lox P cassette containing Exon 2-4 via Cre-mediated recombination. B, Genotype PCR analysis of different tissues that were harvested from 16-week-old *Oc*-Cre;*Pkd1*$^{\text{flox/m1Bei}}$ mice showed bone specific deletion of the *Pkd1* gene. *Osteocalcin*-Cre-mediated recombination of excised floxed *Pkd1* (*Pkd1*$^{\Delta\text{flox}}$) allele occurred exclusively in bone, whereas non-skeletal tissues retained the floxed *Pkd1* allele (*Pkd1*$^{\text{flox}}$). C, Real-time RT-PCR analysis of total *Pkd1* transcripts. Data are expressed as the percentage expression of wild-type (*Pkd1*$^{+}$ and *Pkd1*$^{\text{flox}}$), mutant (*Pkd1*$^{\text{m1Bei}}$), and conditional deleted (*Pkd1*$^{\Delta\text{flox}}$) *Pkd1* alleles for each genotype from 5-6 tibias of 16-week-old mice. Expression of total *Pkd1* transcripts was performed using *Pkd1*-allele-specific primers as described in Experimental Procedures. The normal *Pkd1*$^{+}$ vs cyclophilin A is normalized to the mean ratio of 5 control mice, which has been set to 1. The percentage of conditional deleted and mutant transcripts was calculated from the relative levels of the normal *Pkd1*$^{+}$ transcripts in different *Pkd1* exons. D, Histology of adult kidney. Hematoxylin-eosin (H&E) stained sections from 16-week-old mice failed to identify any cystic tubules in either cortical or medullary regions of kidney from *Oc*-Cre;*Pkd1*$^{\text{flox/+}}$ or *Pkd1*$^{\text{Oc-cko}}$ mice, consistent with the absence of *Oc*-Cre expression in the kidney. In contrast, ablation of *Pkd1* in the kidney caused massive cyst formation, which served as a positive control. Cy, cyst. Scale bars, 100 μm.

FIG. 2. **Cre-mediated somatic loss of *Pkd1* results in loss of bone mass.** A, Effects of *Pkd1*$^{\Delta\text{flox}}$ allele on bone mineral density (BMD) at 16 weeks of age. Similar to Beier *Pkd1* heterozygous mice (*Pkd1*$^{\text{m1Bei/+}}$), there was approximately 7-9% reduction in both male and female of BMD in single excised floxed *Pkd1* heterozygous mice (*Oc*-Cre;*Pkd1*$^{\text{flox/+}}$) compared with age-matched control mice (*Pkd1*$^{\text{flox/+}}$), and an even greater reduction (13-14%) in double heterozygous *Oc*-Cre;*Pkd1*$^{\text{flox/m1Bei}}$ (*Pkd1*$^{\text{Oc-cko}}$) mice, indicating an additive effect of global mutant and conditional deleted *Pkd1* alleles on loss of bone mass. B, Age-dependent effects of *Pkd1*$^{\Delta\text{flox}}$ allele on BMD. Double heterozygous *Pkd1*$^{\text{Oc-cko}}$ mice displayed a significant decrease in femur BMD compared with *Pkd1*$^{\text{m1Bei/+}}$ mice until 16 weeks of age but not at 6 weeks of age, indicating an age-dependent effect of *Pkd1*$^{\Delta\text{flox}}$ allele on bone mass. C, Effects of *Pkd1*$^{\Delta\text{flox}}$ allele on bone structure of femurs. and midshaf diaph. μCT analysis of the distal femoral metaphyses and midshaft diaphyses revealed that double heterozygous *Pkd1*$^{\text{Oc-cko}}$ mice had greater loss in both trabecular and cortical bone than single *Oc*-Cre;*Pkd1*$^{\text{flox/+}}$ and *Pkd1*$^{\text{m1Bei/+}}$ heterozygous mice, consistent with additive effects of global mutant and conditional deleted *Pkd1* alleles on bone structure and a direct role of Pkd1 in bone. Data represent the mean±S.D. from 8-10 individual mice. * indicates significant difference from control (*Pkd1*$^{\text{flox/+}}$), $^{@}$ indicates significant difference from single heterozygous *Oc*-Cre;*Pkd1*$^{\text{flox/+}}$, and $^{\#}$ indicates significant difference from single heterozygous *Oc*-Cre;*Pkd1*$^{\text{flox/+}}$ and *Pkd1*$^{\text{flox/m1Bei}}$ mice at $p<0.05$, respectively.

FIG. 3. **Histological analysis of *Pkd1*$^{\text{Oc-cKO}}$ mice in bone. A**, Goldner and *von Kossa* staining of non-decalcified bone. Representative images of distal femur and lumbar vertebrate sections displayed markedly reductions in trabecular bone volume from 16-week-old *Pkd1*$^{\text{Oc-cko}}$ mice compared with age-matched control mice. Scale bars, 200 μm. B, Bone histomorphometric analyses. There was a significant reduction in periosteal mineral apposition rate (MAR), mineralized surface per bone surface (MS/BS), and bone formation rate (BFR) in single *Oc*-Cre;*Pkd1*$^{\text{flox/+}}$ and *Pkd1*$^{\text{m1Bei/+}}$ heterozygous mice compared with age-matched control *Pkd1*$^{\text{flox/+}}$ mice, and an even greater decrement in double heterozygous *Pkd1*$^{\text{Oc-cko}}$ mice, indicating an additive effect of both global and conditional *Pkd1* deficiency to impair osteoblast-mediated bone formation. Representative images of the distal tibia-fibula junction sections from 16-week-old mice for each genotype showed progressively reductions in the distance between two calcein double-labeling (Scale bars, 20 μm). C, Oil Red O staining of decalcified femur sections. Representative images of femoral bone marrow showed that the number of adipocytes and fat droplets were greater in 18-week-old *Pkd1*$^{\text{Oc-cko}}$ mice compared with age-matched control mice. Scale bars, 100 μm and 500 μm. D, Osmium tetroxide (OsO4) staining of decalcified tibias by μCT analyses. Qualitatively, the images of osmium staining (White or Red area) were much higher in the proximal tibia from 18-week-old *Pkd1*$^{\text{Oc-cko}}$ mice compared with age-matched control mice. Quantification of fat cells number and volume were also performed as described in

Experimental Procedures. Ad.V/Ma.V (%), adipocyte volume/marrow volume; Ad.N (mm^{-3}), adipocyte number (mm^{-3}). Scale bars, 1.0 mm. Data are mean ±S.D. from 3-5 individual mice. * indicates significant difference from control (*Pkd1*$^{\text{flox/+}}$), $^{@}$ indicates significant difference from single heterozygous *Oc*-Cre;*Pkd1*$^{\text{flox/+}}$, and $^{\#}$ indicates significant difference from single heterozygous *Oc*-Cre;*Pkd1*$^{\text{flox/+}}$ and *Pkd1*$^{\text{flox/m1Bei}}$ mice at $p<0.05$, respectively.

FIG 4. ***Pkd1*$^{\text{Oc-cKO}}$ osteoblasts have a developmental defect *ex vivo***. A, BrdU incorporation. Primary cultured *Pkd1*$^{\text{Oc-cKO}}$ osteoblasts exhibited a higher BrdU incorporation than control *Pkd1*$^{\text{flox/+}}$ osteoblasts for 6 hours, indicating increased proliferation in the *Pkd1*$^{\text{Oc-cKO}}$ osteoblasts. B, ALP activity. Primary cultured *Pkd1*$^{\text{Oc-cKO}}$ osteoblasts displayed time-dependent increments in alkaline phosphatase (ALP) activities during 14 days of culture, but the ALP activity was significantly lower at different time points compared with control *Pkd1*$^{\text{flox/+}}$ osteoblasts. C*,* Quantification of mineralization. Alizarin Red-S was extracted with 10% cetylpyridinium chloride and quantified as described in Experimental Procedures. Primary cultured *Pkd1*$^{\text{Oc-cKO}}$ osteoblasts had time-dependent increments in Alizarin Red-S accumulation during 21 days of culture, but the accumulation was significantly lower at different time points compared with control *Pkd1*$^{\text{flox/+}}$ osteoblasts. D, E, Gene expression profiles by real-time RT-PCR. 10-days cultured *Pkd1*$^{\text{Oc-cKO}}$ osteoblasts in osteogenic differentiation media showed a significant attenuation in osteogenesis compared to control osteoblasts, evidenced by a significant reduction in osteoblastic markers including *Osteocalcin* (*Oc*), *Bone sialoprotein (Bsp), Osteopontin (Opn), and Osterix (Osx)*. However, a markedly increase of adipocyte markers such as *PPARγ*, *aP2*, and *Lpl* was observed from the *Pkd1*$^{\text{Oc-cKO}}$ osteoblasts under the same differentiation media when compared with control osteoblasts. Data are mean±S.D. from triple three independent experiments. * indicates significant difference from control (*Pkd1*$^{\text{flox/+}}$) mice at $p<0.05$. Values sharing the same superscript in B and C are not significantly different at $P<0.05$.

FIG 5. **Signaling pathways in *Pkd1*$^{\text{Oc-cKO}}$ osteoblasts.** A, Western blot analysis. Comparison of Akt, GSK3β, and β-catenin expressions in control and *Pkd1*$^{\text{Oc-cKO}}$ osteoblasts treated with or without Wnt3a (100 ηg/ml) for the indicated time. Phosphorylated Akt at Ser473 (panel 1) coincides with phosphorylation of GSK3β at Ser9 (panel 3), reflecting its inactivation by Akt and followed by accumulation of cytoplasmic β-catenin , as detected by Western blot. Total Akt (panel 4), GSK3β (panel 4), and β-actin (panel 6) were used as loading controls for phospho-Akt, phospho-GSK3β and β-catenin in the cytoplasm, respectively. *Pkd1*$^{\text{Oc-cKO}}$ osteoblasts exhibited suppressed activity of the *PI3K-Akt-Gsk3β-β*-catenin signaling pathway under basal and Wnt3a-stimulated conditions. B, TCF/LEF-dependent transcriptional activation as assessed by pTOPFLASH activity. *Pkd1*$^{\text{Oc-cKO}}$ osteoblasts display lower levels of basal TCF/LEF-dependent reporter activity (TOPFLASH) when compared with control *Pkd1*$^{\text{flox/+}}$ osteoblasts. Wnt3a (100 ng/ml) induced reporter activity by more than 2.0-fold above control in *Pkd1*$^{\text{flox/+}}$ osteoblasts, whereas Wnt3a induced reporter activity by only 1.4-fold above control in *Pkd1*$^{\text{Oc-cKO}}$ osteoblasts. C, D, PC1-mediated regulation of *Runx2*-II-P1 prompter activity via PI3K/Akt pathway. Wild-type MC3T3-E1 cells were transiently transfected either control expression vector (sIg∅) or gain-of-function PC1 C-tail construct (PC1-AT) along with the *Runx2*-II-P1 luciferase reporter (p0.42*Runx2*-P1-Luc) construct in the presence or absence of PI3K inhibitor LY294002 or dn-*Akt* construct. PC1-mediated activation of *Runx2*-II-P1 promoter activity was dose-dependently diminished by either PI3K inhibitor LY294002 or dn-*Akt* construct. E, Gene expression profiles by real-time RT-PCR. 10-days cultured *Pkd1*$^{\text{Oc-cKO}}$ osteoblasts in differentiation media showed a significant attenuation in Wnt/β-catenin signaling compared to control osteoblasts, evidenced by a significant down-regulation of Wnt/β-catenin targeting genes including *Wnt10b*, *Axin2*, *Cox2* and *Runx2*-II, and up-regulation of its antagonist genes such as *sFrp1* and *sFrp4*. Data are mean±S.D. from triple independent experiments. * indicates significant difference from control (*Pkd1*$^{\text{flox/+}}$) mice at $p<0.05$. Values sharing the same superscript in C and D are not significantly different at $P<0.05$.

TABLE I *Gene-expression profiles in 16-week-old mice*

Gene	Accession no.	*Oc*-Cre;*Pkd1*$^{flox/+}$	*Pkd1*$^{flox/m1Bei}$	*Oc*-Cre;*Pkd1*$^{flox/m1Bei}$	*p*-value
Osteoblast lineage					
*Runx*2-II	NM_009820	0.73±0.04*	0.71±0.08*	0.45±0.07*$^{,\#}$	0.0007
*Runx*2-I	D14636	1.14±0.32	1.16±0.14	1.15±0.18	0.5961
*Runx*2	NM_009820	0.73±0.09*	0.71±0.16*	0.51±0.07*$^{,\#}$	0.0009
Osteocalcin	NM_007541	0.82±0.12*	0.80±0.11*	0.46±0.08*$^{,\#}$	<0.0001
Osteopontin	AF515708	0.73±0.11*	0.69±0.11*	0.44±0.03*$^{,\#}$	0.0027
Bsp	NM_008318	0.73±0.07*	0.71±0.08*	0.52±0.06*$^{,\#}$	<0.0001
Opg	MMU94331	0.71±0.15*	0.70±0.11*	0.68±0.20*	0.0295
Rank ligand	NM_011613	0.70±0.12*	0.57±0.07*	0.39±0.07*$^{,\#}$	<0.0001
Mmp13	NM_008607	0.97±0.16	0.65±0.05*	0.43±0.11*$^{,\#}$	<0.0001
Dmp1	MMU242625	0.71±0.06*	0.64±0.12*	0.40±0.05*$^{,\#}$	<0.0001
Phex	NM_011077	0.72±0.12*	0.67±0.12*	0.58±0.14*	0.0002
Osteoclast					
Trap	NM_007388	0.68±0.11*	0.63±0.13*	0.36±0.09*$^{,\#}$	<0.0001
*Mmp*9	NM_013599	0.95±0.16	0.69±0.08*	0.63±0.07*	0.0001
Chondrocyte					
Collagen II	NM_031163	0.99±0.13	1.03± 0.26	1.13±0.23	0.5764
VegfA	NM_009505	1.07±0.26	1.06± 0.21	0.97±0.31	0.8905
Adipocyte					
PPARγ	NM_009505	1.08±0.15	1.20± 0.19	1.40±0.13*	0.0025
aP2	NM_024406	1.13±0.16	1.55± 0.23*	1.95±0.26*$^{,\#}$	<0.0001
Lpl	NM_008509	1.38±0.25*	1.42± 0.27*	2.01±0.29*$^{,\#}$	<0.0001
Others					
IFNγ	NM_008337	2.42±0.79*	2.70± 1.21*	3.57±1.51*	0.0039
TNFα	NM_013693	1.18±0.32	1.23± 0.69	1.13±0.39	0.8371
TRAIL	NM_009425	1.36±0.51	1.33± 0.48	1.29±0.45	0.4500
Alox15	NM_009660	1.93±0.38*	2.22± 0.89*	2.40±0.95*	0.0106

Data are mean ±S.D. from 5-6 tibias of 6-week-old individual mice and expressed as the fold changes relative to the housekeeping gene *cyclophilin* A subsequently normalized to control (*Pkd1*$^{flox/+}$) mice. *indicates significant difference from control (*Pkd1*$^{flox/+}$), and $^{\#}$ indicates significant difference from single heterozygous *Oc*-Cre;*Pkd1*$^{flox/+}$ and *Pkd1*$^{flox/m1Bei}$ mice at $p<0.05$, respectively.

TABLE II *Biochemistry analysis of serum in 16-week-old mice*

Genotype	*Pkd1*$^{flox/+}$	*Oc*-Cre;*Pkd1*$^{flox/+}$	*Pkd1*$^{flox/m1Bei}$	*Oc*-Cre;*Pkd1*$^{flox/m1Bei}$
BUN(mg/dl)	19±4.9	20±4.8	22±4.3	22±5.2
Ca (mg/dl)	8.9±0.27	8.7±0.38	8.6±0.34	8.5±0.37
P (mg/dl)	8.3±0.95	8.5±1.17	8.6±1.50	8.8±0.76
Osteocalcin (ηg/ml)	87±21.3	74±13.8*	64±18.6*	56±12.6$^{*,\#}$
TRAP (U/L)	12.6±4.54	8.0±2.94*	6.5±1.61*	5.1±0.94$^{*,\#}$

Data are mean ±S.D. from 9 individual mice. * indicates significant difference from control (*Pkd1*$^{flox/+}$), and $^{\#}$ indicates significant difference from single heterozygous *Oc*-Cre;*Pkd1*$^{flox/+}$ and *Pkd1*$^{flox/m1Bei}$ mice at $p<0.05$, respectively. Osteocalcin is produced by osteoblasts, and TRAP is produced by osteoclasts.

Figure 1

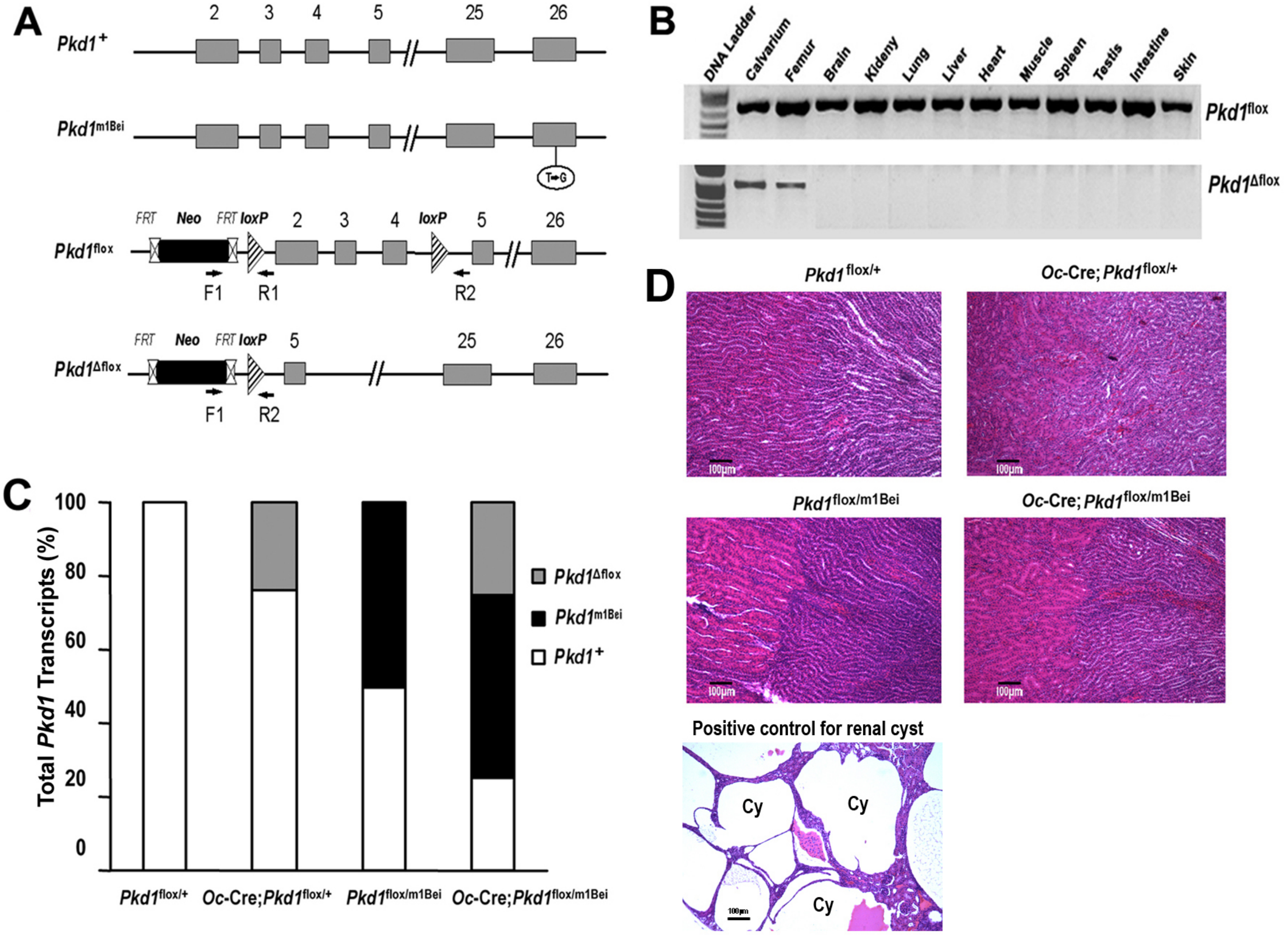
A
Pkd1+
2
3
4
5
25
26
Pkd1m1Bei
T→G
Pkd1flox
FRT
Neo
FRT
loxP
loxP
F1
R1
R2
Pkd1Δflox
F1
R2
B
DNA Ladder
Calvarium
Femur
Brain
Kidney
Lung
Liver
Heart
Muscle
Spleen
Testis
Intestine
Skin
Pkd1flox
Pkd1Δflox
C
Total Pkd1 Transcripts (%)
100
80
60
40
20
0
Pkd1Δflox
Pkd1m1Bei
Pkd1+
Pkd1flox/+
Oc-Cre;Pkd1flox/+
Pkd1flox/m1Bei
Oc-Cre;Pkd1flox/m1Bei
D
Pkd1 flox/+
Oc-Cre; Pkd1flox/+
Pkd1flox/m1Bei
Oc-Cre; Pkd1flox/m1Bei
100μm
Positive control for renal cyst
Cy
Cy
Cy

Figure 2

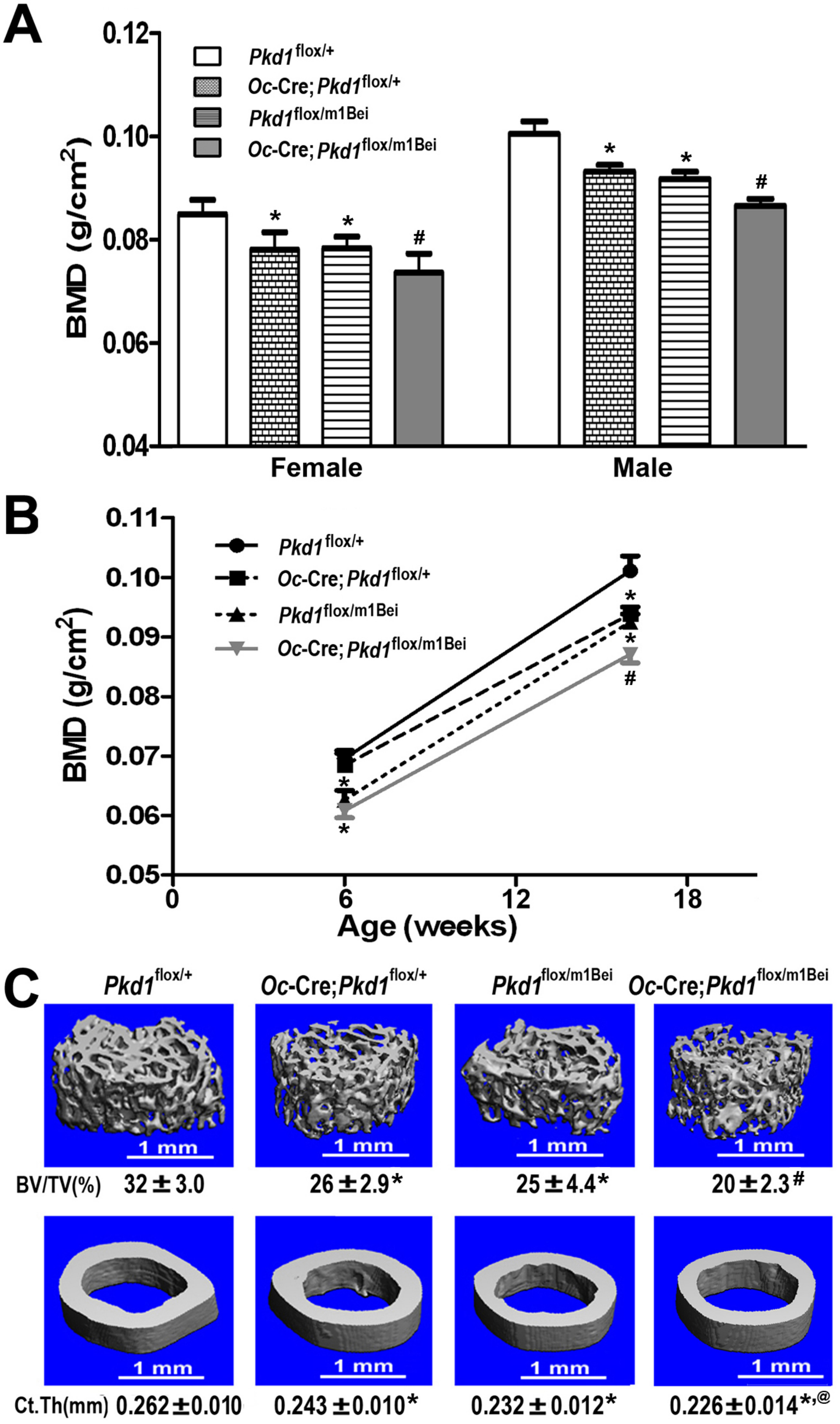
A
BMD (g/cm²)
0.12
0.10
0.08
0.06
0.04
Pkd1 flox/+
Oc-Cre; Pkd1 flox/+
Pkd1 flox/m1Bei
Oc-Cre; Pkd1 flox/m1Bei
*
*
#
*
*
#
Female
Male
B
BMD (g/cm²)
0.11
0.10
0.09
0.08
0.07
0.06
0.05
0
6
12
18
Age (weeks)
Pkd1 flox/+
Oc-Cre; Pkd1 flox/+
Pkd1 flox/m1Bei
Oc-Cre; Pkd1 flox/m1Bei
*
*
*
*
#
C
Pkd1 flox/+
Oc-Cre;Pkd1 flox/+
Pkd1 flox/m1Bei
Oc-Cre;Pkd1 flox/m1Bei
1 mm
BV/TV(%)
32 ± 3.0
26 ± 2.9*
25 ± 4.4*
20 ± 2.3#
Ct.Th(mm)
0.262 ± 0.010
0.243 ± 0.010*
0.232 ± 0.012*
0.226 ± 0.014*,@

Figure 3

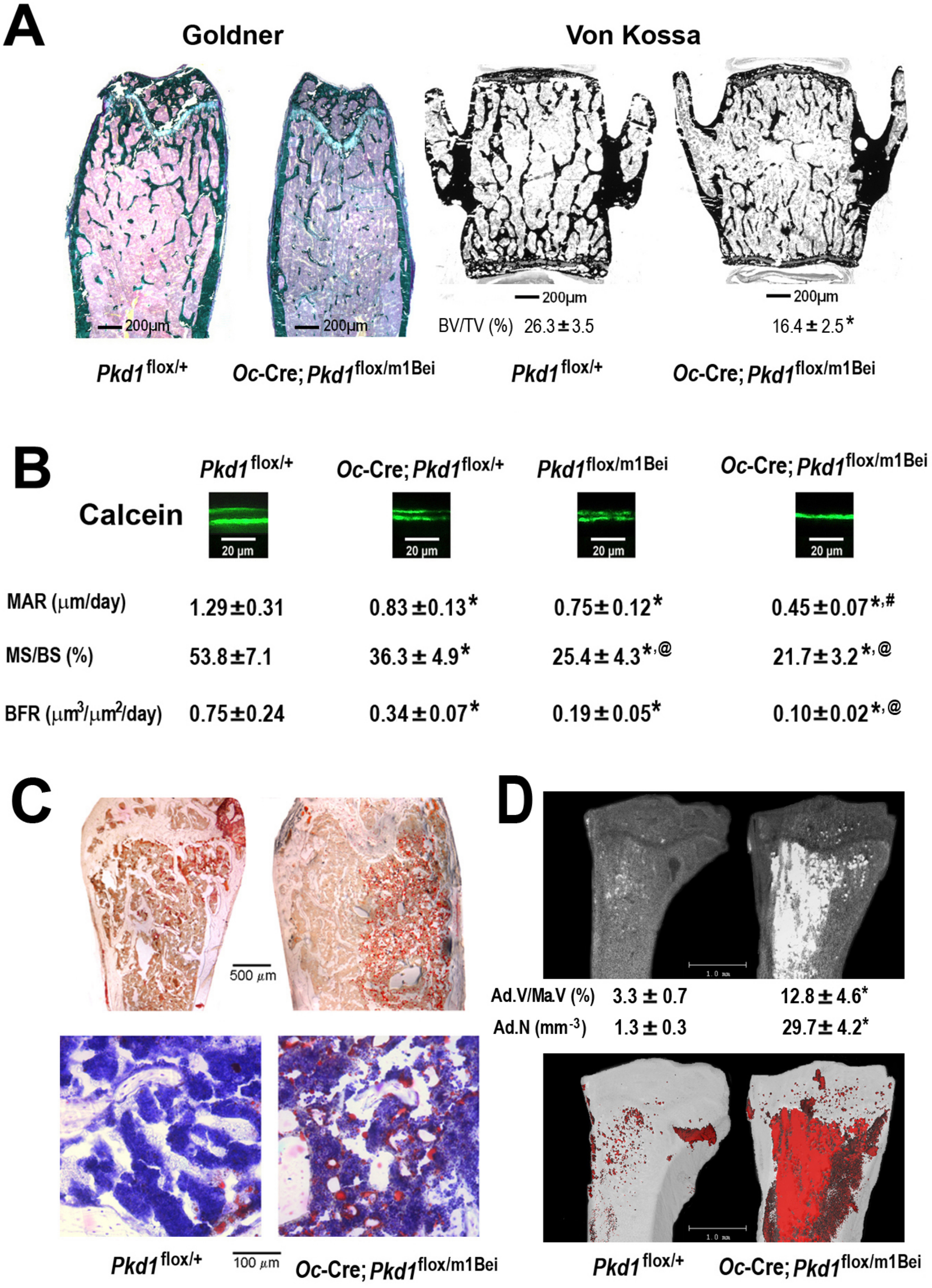

	Pkd1 flox/+	*Oc*-Cre; *Pkd1* flox/+	*Pkd1* flox/m1Bei	*Oc*-Cre; *Pkd1* flox/m1Bei
MAR (µm/day)	1.29±0.31	0.83±0.13*	0.75±0.12*	0.45±0.07*,#
MS/BS (%)	53.8±7.1	36.3±4.9*	25.4±4.3*,@	21.7±3.2*,@
BFR ($\mu m^3/\mu m^2$/day)	0.75±0.24	0.34±0.07*	0.19±0.05*	0.10±0.02*,@

	Pkd1 flox/+	*Oc*-Cre; *Pkd1* flox/m1Bei
Ad.V/Ma.V (%)	3.3 ± 0.7	12.8 ± 4.6*
Ad.N (mm^{-3})	1.3 ± 0.3	29.7± 4.2*

Figure 4

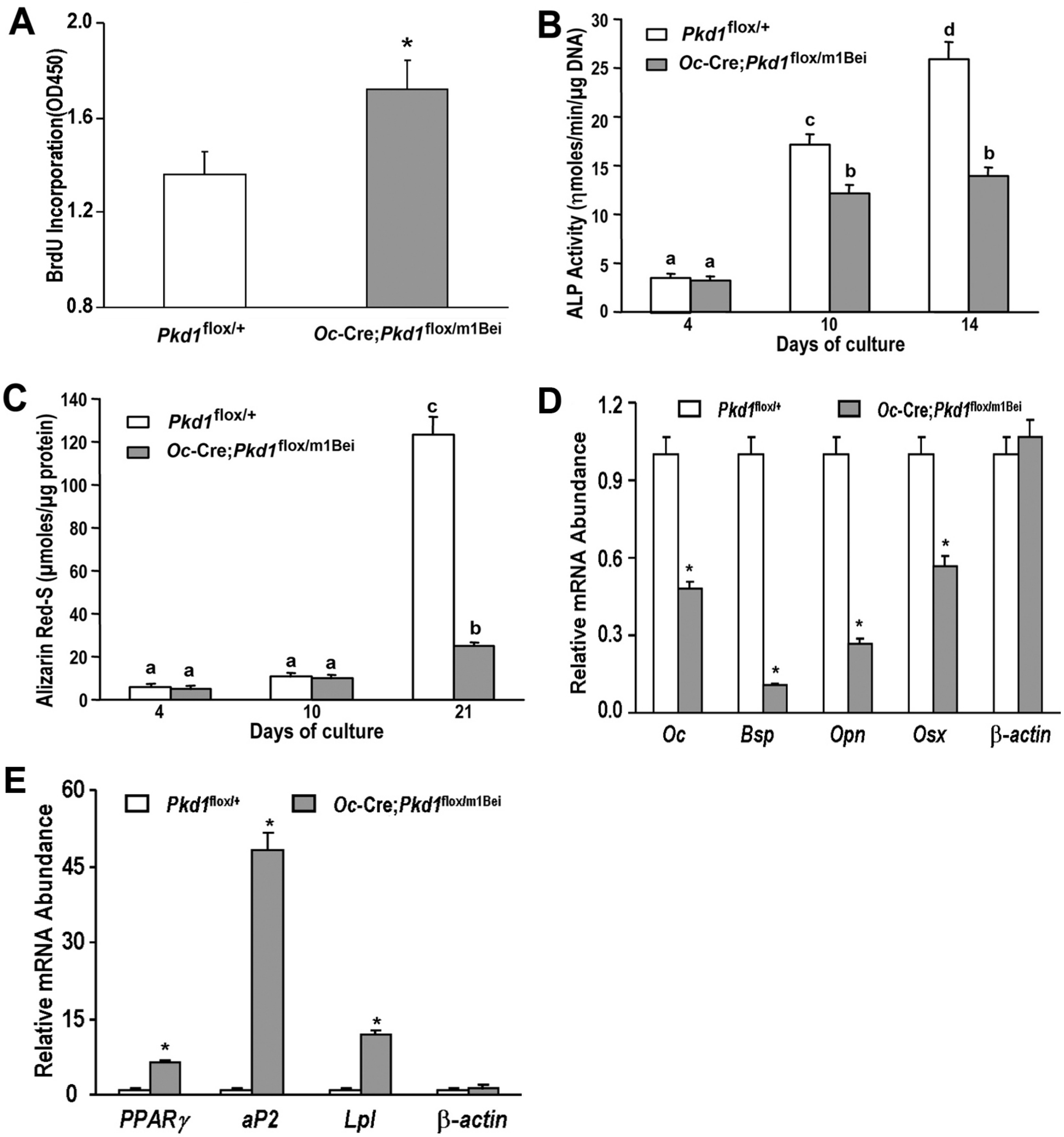
A
BrdU Incorporation(OD450)
2.0
1.6
1.2
0.8
*
Pkd1$^{flox/+}$
Oc-Cre;Pkd1$^{flox/m1Bei}$
B
ALP Activity (ηmoles/min/μg DNA)
30
25
20
15
10
5
0
Pkd1$^{flox/+}$
Oc-Cre;Pkd1$^{flox/m1Bei}$
a
a
c
b
d
b
4
10
14
Days of culture
C
Alizarin Red-S (μmoles/μg protein)
140
120
100
80
60
40
20
0
Pkd1$^{flox/+}$
Oc-Cre;Pkd1$^{flox/m1Bei}$
a
a
a
a
c
b
4
10
21
Days of culture
D
Relative mRNA Abundance
1.2
0.9
0.6
0.3
0.0
Pkd1$^{flox/+}$
Oc-Cre;Pkd1$^{flox/m1Bei}$
*
*
*
*
Oc
Bsp
Opn
Osx
β-actin
E
Relative mRNA Abundance
60
45
30
15
0
Pkd1$^{flox/+}$
Oc-Cre;Pkd1$^{flox/m1Bei}$
*
*
*
PPARγ
aP2
Lpl
β-actin

Figure 5

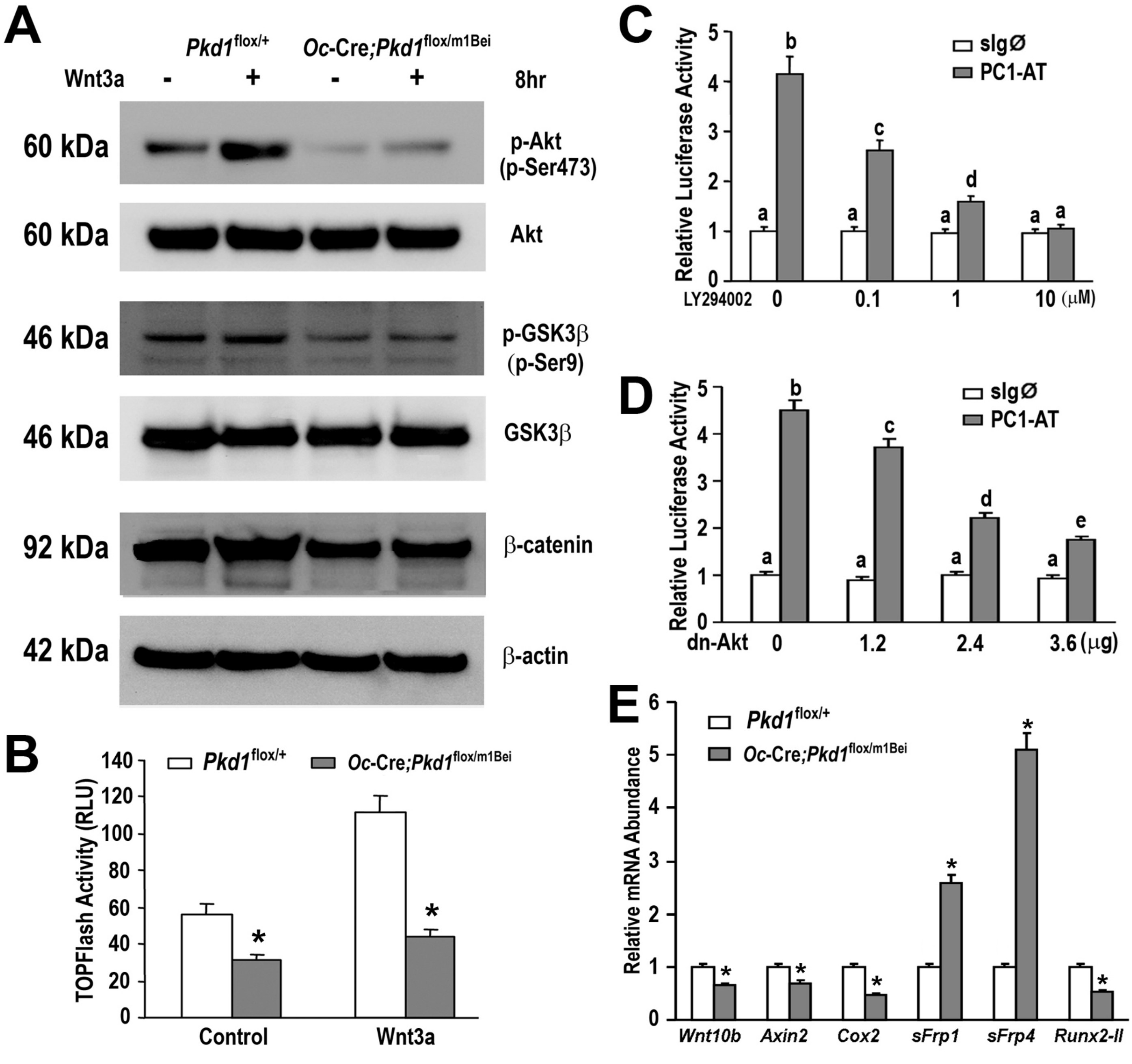
A
Pkd1flox/+
Oc-Cre;Pkd1flox/m1Bei
Wnt3a - + - + 8hr
60 kDa
p-Akt (p-Ser473)
60 kDa
Akt
46 kDa
p-GSK3β (p-Ser9)
46 kDa
GSK3β
92 kDa
β-catenin
42 kDa
β-actin
B
Pkd1flox/+
Oc-Cre;Pkd1flox/m1Bei
TOPFlash Activity (RLU)
0
20
40
60
80
100
120
140
*
*
Control
Wnt3a
C
sIgØ
PC1-AT
Relative Luciferase Activity
0
1
2
3
4
5
a b a c a d a a
LY294002 0 0.1 1 10 (μM)
D
sIgØ
PC1-AT
Relative Luciferase Activity
0
1
2
3
4
5
a b a c a d a e
dn-Akt 0 1.2 2.4 3.6 (μg)
E
Pkd1flox/+
Oc-Cre;Pkd1flox/m1Bei
Relative mRNA Abundance
0
1
2
3
4
5
6
* * * * * *
Wnt10b
Axin2
Cox2
sFrp1
sFrp4
Runx2-II